DESIGN OF ELLIPTIC-FUNCTION-TYPE E-PLANE FILTERS FOR MILLIMETER-WAVE APPLICATIONS

Jens Bornemann

ABSTRACT

An efficient and rigorous modal S-matrix method for the design of elliptic-function type E-plane filters is introduced. By supplementing conventional metal insert filters with inductively coupled stopband sections, the component achieves both, improved skirt selectivity and compatibility with millimeter-wave intregated circuit manufacturing processes. The theoretical treatment includes the finite strip thickness of the insert as well as higher-order mode interactions at all discontinuities involved. Ka-band structures with two and four attenuation peak responses are presented as design examples.

ZUSAMMENFASSUNG

Es wird eine effiziente und strikte modale S-Matrix Methode zum Entwurf von E-Ebenen Filtern, die dem Typ elliptischer Funktionen-Filter entsprechen, vorgestellt. Durch die Ergänzung konventioneller Metallstegfilter mit induktiv gekoppelten Sperrbereichsgliedern erreicht diese Komponente sowohl verbesserte Flankensteilheit als auch Kompatibilität mit dem Herstellungsverfahren von integrierten Millimeterwellen-Schaltungen. Die theoretische Formulierung beinhaltet die endliche Metallisierungsstärke des Einsatzes wie auch die gegenseitige Beeinflussung von Moden höherer Ordnung an sämtlichen Diskontinuitäten. Als Entwurfsbeispiele werden Ka-Band-Strukturen mit zwei- und vierfachen Dämpfungsspitzen präsentiert.

1. INTRODUCTION

Channel selecting or separating networks, such as input and output multiplexers, often require filter components with extremely high skirt selectivity, e.g. [1]-[3]. At microwave frequencies, common realizations comprise iris-coupled circular waveguide cavities [4] or dielectric loaded circular waveguides [5, 6], both in dual-mode operation. These designs, however, require tuning and/or coupling adjusting screws which are appropriate at microwave frequencies but which will certainly lead to difficulties in case of millimeter-wave applications, when the tuning screw diameter (e.g. 1mm) approaches the waveguide cross-sectional dimensions (W-band height = 1.27mm). Therefore, different technologies must be used for high skirt selectivity filters in the millimeter-wave range.

Here, all-metal insert E-plane integrated circuit filters [7] are well established low-cost, low-loss and mass-producible components. Numerical design calculations [8] are in extremely close agreement with measurements (up to 150 GHz) [9], and steps have been taken to improve the passband separation as well as the stopband attenuation [10, 11]. Achieving higher selectivity with these filters, however, is difficult. Increasing the number of resonators usually leads to higher insertion loss [12], and metal insert filters are not suitable for dual-mode operation. One way to accomplish improved skirt selectivity, though, is to add stopband circuits which can provide attenuation peaks in the overall frequency response. This can be achieved by mounting slot- or iris-coupled waveguide resonators on top of the filter housing [13]. A different approach using two-path cutoff waveguide dielectric resonator filters is proposed in [14]. However, none of these structures is suitable for E-plane integrated circuit fabrication.

Recently, a new E-plane metal insert filter design concept has been introduced [20], which accomplishes both, improved skirt selectivity and E-plane compatibility with the millimeter-wave integrated circuit manufacturing process. Since the attenuation peaks in the bandpass response are obtained using inductively coupled waveguide resonators rather than slot-coupled cavities, the planar filter structure etched from a metal foil can be sandwiched between the two parts of a waveguide split-block housing (Fig. 1).

This contribution focusses on the computer-aided design procedure for elliptic-function-type E-plane filters. Based on a numerical description of the electromagnetic field within the structure, the mode-matching technique is applied to include higher-order mode interactions and the influence of the finite strip thickness. The design is carried out by numerically analyzing a configuration while its parameters are varied by an optimization routine until a specified filter response is obtained [12]. Due to the fact that only the modelling of the discontinuities rather than the homogeneous waveguide sections requires a large number of higher order modes during the analysis, the design software is fully operational on modern 386-type personal computers.

Department of Electrical and Computer Engineering, University of Victoria, P.O. Box 1700, Victoria, B.C., Canada V8W 2Y2, Tel: (604) 721-8666

2. THEORY

The field theory treatment of the elliptic-function-type E-plane filter structure is based on a selected-mode scattering matrix analysis. The utilized superposition of longitudinal-section TE^z_{mo} modes (waveguide bi-furcation [8, 9]) and TE^z_{1n} modes (E-plane T-junction [15]) requires the electric field components in x-direction to be zero. Provided that the component is operated in the monomode range of the waveguide housing, then the above assumption is virtually true if $d_3, \ell_0, \ell_N, d_6 > b$ (c.f. Fig. 1).

Hence the resulting five field components of the TE^z_{mn}-mode spectrum may be derived from the vector potential $\vec{A}_h = A_{hz}\vec{e}_z$

$$\begin{aligned} \vec{E} &= \nabla \times (A_{hz}\vec{e}_z) \\ \vec{H} &= \frac{j}{w\mu} \nabla \times \nabla \times (A_{hz}\vec{e}_z) \quad , \end{aligned} \tag{1}$$

which is expressed in terms of the eigenfunctions of the individual homogeneous subregions:

$$\begin{aligned} A_{hz} = &\sum_{m=1}^{M} \sum_{n=0}^{N} A_{mn} \sin(k_{xm}x) \frac{\cos(n\pi y/b)}{\sqrt{1+\delta_{on}}} \\ &\cdot [V_{mn} \exp(-jk_{zmn}z) - R_{mn} \exp(+jk_{zmn}z)] \end{aligned} \tag{2}$$

In (2), δ_{on} is the Kronecker delta, V_{mn} and R_{mn} are the amplitudes of forward and backward traveling waves, respectively, k_{zmn} is the related propagation constant in that subregion, and k_{xm} equals $2m\pi/(a-t)$ in metal insert sections or $(2m-1)\pi/a$ in waveguide sections to account for the $y-z$-symmetry plane at $x = a/2$ (Fig. 1). A_{mn} is a power normalization term which is required to satisfy the general modal scattering matrix relations outlined in [16].

Although the choice of the same waveguide height b for the filter section ($\ell_0 - \ell_N$) as well as the E-plane stubs ($d_1 - d_6$) is not a restriction for the field theory description, two design considerations are favorable associated with the pre-specification of these parameters: First, the computation time is considerably reduced, since the modal scattering matrix for the bi-furcation can be used for both the filter and the stub sections by exchanging y and z in (2). Hence this part of the calculation need be computed only once. Second, the unloaded Q's of stubsection and filter resonators are identical since the same waveguide cross-section is used.

In order to analyse the overall filter response, general mode matching techniques are used. Since the modal scattering matrices of connecting homogeneous media of different cross-sections and those of resonator regions formed by T-junctions have already been presented in [16] and [17] respectively, only the formulas to be computed for the present configuration are given in this section.

a) Waveguide bi-furcation

Since the filter structure is symmetrical with respect to $x = a/2$, the waveguide bi-furcation discontinuity can be described by the modal scattering matrix ($\underline{S}_D$) of a two-port.

$$\begin{aligned} \underline{S}_{D11} &= [\underline{L}_E\underline{L}_H + \underline{I}]^{-1}[\underline{L}_E\underline{L}_H - I] \\ \underline{S}_{D12} &= 2[\underline{L}_E\underline{L}_H + \underline{I}]^{-1}\underline{L}_E \\ \underline{S}_{D21} &= \underline{I} - \underline{S}_{D11} \\ \underline{S}_{D22} &= I - \underline{L}_H\underline{S}_{D12} \end{aligned} \tag{3}$$

In (3), $\underline{I}$ is the unit matrix and the elements of matrices $\underline{L}_E$, $\underline{L}_H$ are given by

$$\begin{aligned} (\underline{L}_E)_{mn,kn} &= 4 \sqrt{\frac{k^{II}_{zkn}[k_0^2 - (k^I_{xm})^2]}{a\frac{a-t}{2}k^I_{zmn}[k_0^2 - (k^{II}_{xk})^2]}} \\ &\quad \cdot \int_0^c \sin(k^I_{xm}x)\sin(k^{II}_{xk}x)dx \end{aligned} \tag{4}$$

$$(\underline{L}_H) = \frac{1}{2}(\underline{L}_E)^T \quad (T \triangleq \text{ transposed}), \tag{5}$$

$$k^I_{xm} = (2m-1)\frac{\pi}{a}, \quad k^{II}_{xk} = \frac{k\pi}{c},\ c = \frac{a-t}{2} \tag{6}$$

$$\begin{aligned} k^I_{zmn} &= \sqrt{k_0^2 - (k^I_{xm})^2 - \left(\frac{n\pi}{b}\right)^2} \\ k^{II}_{zkn} &= \sqrt{k_0^2 - (k^{II}_{xk})^2 - \left(\frac{n\pi}{b}\right)^2} \\ k_o &= 2\pi f\sqrt{\mu_0\epsilon_0} \end{aligned} \tag{7}$$

Combinations of integers mn, kn in (4) are assigned one matrix element, e.g. $(\underline{L}_E)_{i,j}$.

b) Metal insert of finite length

The modal scattering matrix ($\underline{S}_M$) of the metal insert of finite length ℓ_i can be calculated by using (3) for both discontinuities. As a result, the following submatrices are obtained.

$$\begin{aligned} \underline{S}_{M11} &= \underline{S}_{M22} = \underline{S}_{D11} + \underline{S}_{D12}\,\underline{R}^{II}\,\underline{S}_{D22}\,\underline{W}\,\underline{R}^{II}\,\underline{S}_{D21} \\ \underline{S}_{M12} &= \underline{S}_{M21} = \underline{S}_{D12}\,\underline{W}\,\underline{R}^{II}\,\underline{S}_{D21} \end{aligned} \tag{8}$$

$$\text{with} \quad \underline{W} = [\underline{I} - \underline{R}^{II}\underline{S}_{D22}\,\underline{R}^{II}\,\underline{S}_{D22}]^{-1} \tag{9}$$

$$\text{and} \quad \underline{R}^{II} = \text{Diag}\,\{\exp(-jk^{II}_{zkn}\cdot\ell_i)\} \tag{10}$$

The diagonal elements of $\underline{R}^{II}$ are again formed by combinations of kn.

c) Input reflection matrix of E-plane stubs

The input reflection matrix $\underline{S}_{S11}$ of the E-plane stubs $d_1 - d_3$ (c.f. Fig. 1) is computed by replacing ℓ_i by d_2 in (8) - (10), and by using the modal scattering submatrix $\underline{R}_{SC}$ and the submatrix of the empty waveguide section $\underline{R}^I$ of length d_3.

$$\begin{aligned} \underline{R}_{SC} &= \text{Diag}\,\{-\exp(-j2k^I_{zmn}d_1)\} \\ \underline{R}^I &= \text{Diag}\,\{\exp(-jk^I_{zmn}d_3)\} \end{aligned} \tag{11}$$

Then $\underline{S}_{S11}$ is given by

$$\underline{S}_{S11} = \underline{R}^I\,\{\underline{S}_{M11} + \underline{S}_{M12}\,\underline{R}_{SC}[\underline{I} - \underline{S}_{M22}\,\underline{R}_{SC}]^{-1}\underline{S}_{M21}\}\underline{R}^I, \tag{12}$$

which, of course, holds for the second stub section when $d_1 - d_3$ is replaced by $d_4 - d_6$.

d) Stopband section

A stopband section consists of one T-junction and one E-plane stub. The resulting circuit is a two-port with modal scattering submatrices given by

$$\begin{aligned} \underline{S}_{G11} &= \underline{S}_{G22} = \underline{S}_{11} + \underline{S}_{13}\underline{S}_{S11}[\underline{I} - \underline{S}_{33}\underline{S}_{S11}]^{-1}\underline{S}_{31} \\ \underline{S}_{G21} &= \underline{S}_{G12} = \underline{S}_{21} + \underline{S}_{23}\underline{S}_{S11}[\underline{I} - \underline{S}_{33}\underline{S}_{S11}]^{-1}\underline{S}_{31}, \end{aligned} \tag{13}$$

where $\underline{S}_{S11}$ is given by (12), and $\underline{S}_{ik}$ are the submatrices of the three-port waveguide T-junction given in the Appendix.

Finally, the two-port matrices of the symmetrical filter sections ($\ell_i = \ell_{N-i}$) and the stopband sections are successively combined by an algorithm requiring only one matrix inversion per cascaded two-port [18].

In the computer analysis only the two general discontinuities involved are calculated with up to $M = 45$ and $N = 25$ modes. In detail, the following modes are selected: $TE^z_{1,0}$ to $TE^z_{45,0}$ and $TE^z_{1,1}$ to $TE^z_{1,4}$ for the waveguide bi-furcation (eqns. 3 - 7); and $TE^z_{1,0}$ to $TE^z_{9,0}$ and $TE^z_{1,1}$ to $TE^z_{1,25}$ for the T-junction. For all S-matrix combining algorithms, however, only the lowest 9 modes are selected (5 types of the $TE^z_{m,0}$-mode spectrum and additional 4 types of the $TE^z_{1,n}$-mode spectrum). Due to the basic five field component assumption ($d_3, \ell_0, \ell_N, d_6 > b$), this procedure provides results within the plotting accuracy compared with a full-mode analysis, e.g. [19], and allows the software to be operational on 386-type personal computers, where at a clock rate of 20 MHz approximately five minutes are required for one set of input parameters.

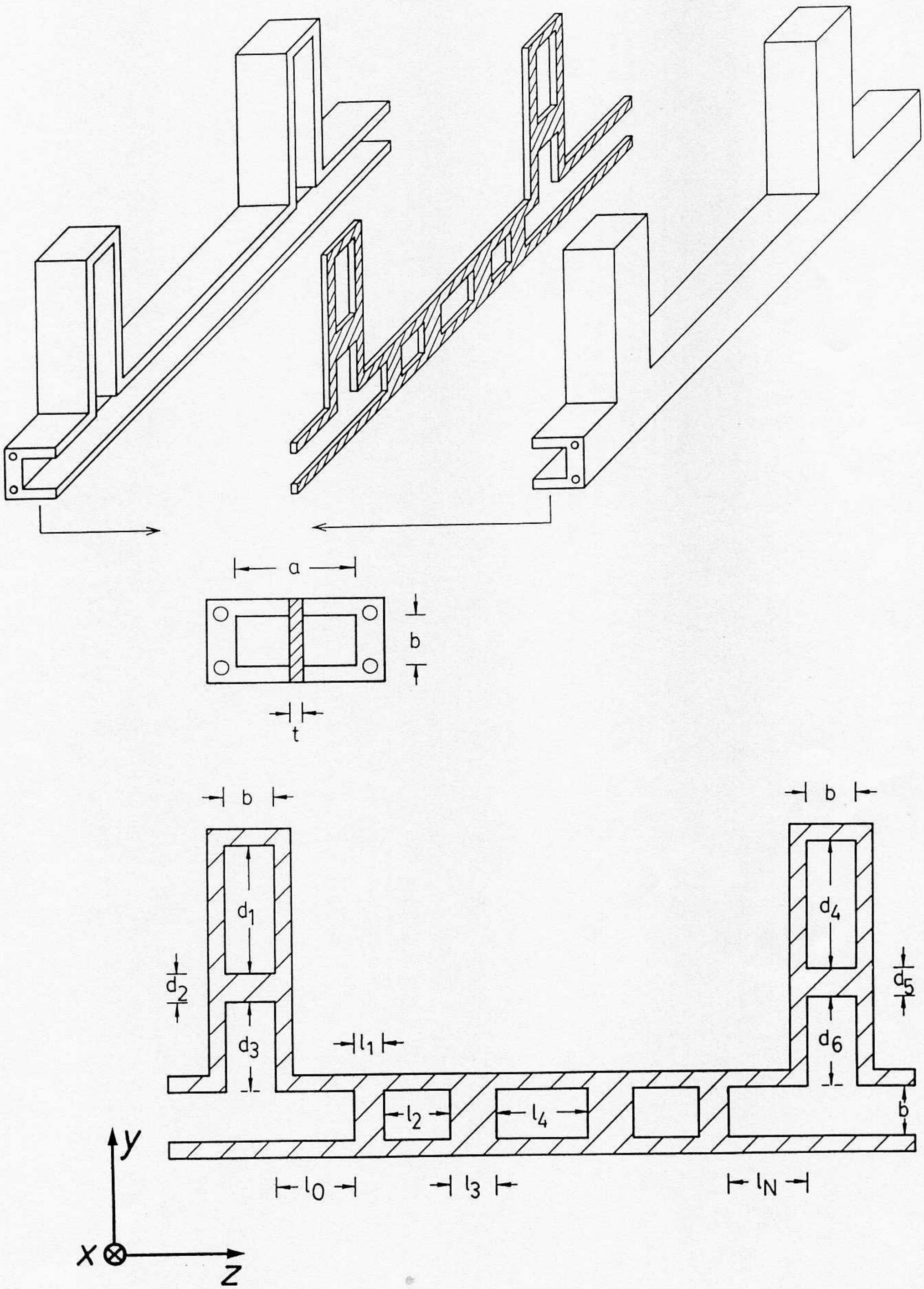

Figure 1
Millimeter-wave E-plane filter with elliptic-function-type response

3. DESIGN

Rather than optimizing the structure as a whole, the following procedure has turned out to be efficient and reliable for the design of elliptic-function-type E-plane filters.

a) Design of the filter section ($\ell_1 - \ell_{N-1}$) by using the optimization method described in [12].

b) Design of the stopband section by setting d_1 as well as $d_3 + b$ equal to the guide wavelength at midband frequency. The coupling section d_2 should be made as short as possible. This value usually falls in the order of magnitude of the strip thickness. Due to the influence of the strip, the final values of d_1 and $d_3 + b$ are slightly lower than one wavelength.

c) With the dimensions obtained in steps a and b the complete structure is designed by varying ℓ_0 and ℓ_N only. Usually, $\ell_0 = \ell_N$ is a good choice.

It should be noted that no optimization strategy is necessary for steps b and c. A final optimization run, however, provides better return loss responses.

4. DESIGN EXAMPLES

As has been shown in [20], one stopband section can produce two attenuation peaks in the filter response if tight coupling (d_2, d_5 in the order of magnitude of the strip thickness) is used. A Ka-band example with identical stopband sections is presented in Fig. 2. Although the conventional metal insert filter (dashed lines) shows slightly better performance in the vicinity of the passband, the attenuation peaks of the elliptic-function-type design (solid lines) significantly improve the skirt selectivity of the component while maintaining an acceptable return loss behavior.

For more narrow-band applications, the attenuation peaks need to come closer to the filter band edges. This solution is presented in Figs. 3. By selecting different midband frequencies for the two stopband stubs (Fig. 3, top) one attenuation peak of either stub approaches the filter passband at 33 GHz. As a result, Fig. 3 (bottom) presents the four-peak filter response obtained. Due to the finite bandwidth of the stopband sections, however, the passband ripple is increased significantly to 1.6 dB compared with an approximately flat response of the conventional filter type. Therefore, it is recommended that the application of the elliptic-function-type E-plane filters presented here be restricted to bandwidths greater than one percent.

5. CONCLUSIONS

An efficient modal scattering matrix procedure for the design of elliptic-function-type E-plane filters has been presented. Since only the significant modes are selected to describe the actual electromagnetic field within the structure, the design software is operational on modern personal computers. The structure itself is compatible with millimeter-wave integrated circuit manufacturing processes and is expected to be well suited for applications up to 100 GHz. Ka-band design examples demonstrate the superiority of the elliptic-function-type design when compared with its conventional counterpart.

APPENDIX

Submatrices $\underline{S}_{ik}$ in (13):

For this application where the three ports have identical cross-sections, the calculation of the general scattering matrix of the T-junction can be simplified. Assuming that port 3 is pointing in the y-direction (Fig. 1), the following identities are obtained:

$$\underline{S}_{11} = \underline{S}_{22},\ \underline{S}_{13} = \underline{S}_{23} = \underline{S}_{31} = \underline{S}_{32},\ \underline{S}_{21} = \underline{S}_{12}$$

Hence, only $\underline{S}_{11}$, $\underline{S}_{13}$, $\underline{S}_{21}$ and $\underline{S}_{33}$ need to be calculated to compute the stopband section scattering matrices in (13).

$$\begin{aligned}
\underline{S}_{11} &= -[\underline{D}_S\,\underline{A} + \underline{L}^I\,\underline{U} - \underline{D}_T + \underline{I}]^{-1} \\
&\quad [\underline{D}_S\,\underline{A} + \underline{L}^I\,\underline{U} - \underline{D}_T - \underline{E}] \\
\underline{S}_{13} &= -[\underline{D}_S\,\underline{A} + \underline{L}^I\underline{U} - \underline{D}_T + \underline{I}]^{-1}[\underline{D}_S\,\underline{C} + \underline{L}^I(\underline{B} + \underline{I})] \\
\underline{S}_{21} &= \underline{A}[\underline{S}_{11} + \underline{I}] \\
\underline{S}_{33} &= \underline{U}\,\underline{S}_{13} + \underline{B}
\end{aligned}$$

Here, $\underline{I}$ is the unit matrix and

$$\begin{aligned}
\underline{A} &= \underline{V}\{\underline{L}^{II}[\underline{I} - \underline{D}_T]^{-1}\underline{L}^{III} - \underline{D}_S\} \\
\underline{B} &= \underline{V}\{\underline{I} + \underline{D}_T + \underline{L}^{II}[\underline{I} - \underline{D}_T]^{-1}\underline{L}^{II}\} \\
\underline{C} &= \underline{V}\,\underline{L}^{II}\{\underline{I} + [\underline{I} - \underline{D}_T]^{-1}[\underline{I} + \underline{D}_T]\} \\
\underline{U} &= \underline{V}\{\underline{L}^{III} - \underline{L}^{II}[\underline{I} - \underline{D}_T]^{-1}\underline{D}_S\} \\
\underline{V} &= \{\underline{I} - \underline{D}_T - \underline{L}^{II}[\underline{I} - \underline{D}_T]^{-1}\underline{L}^{II}\}^{-1}
\end{aligned}$$

The coupling matrices $\underline{L}^I - \underline{L}^{III}$ are given by

$$(\underline{L}^I)_{mn,mi} = \frac{2j/b}{\sin(k^I_{zmi}b)}\sqrt{k^I_{zmn}/k^I_{zmi}} \cdot \int_0^b \frac{\cos(n\pi y/b)}{\sqrt{1+\delta_{on}}}\,\frac{\cos(k^I_{zmi}y)}{\sqrt{1+\delta_{oi}}}\,dy$$

$$(\underline{L}^{II})_{mn,mi} = (-1)^i(\underline{L}^I)_{mn,mi}$$

$$(\underline{L}^{III})_{mn,mi} = \frac{-2j/b}{\sin(k^I_{zmi}b)}\sqrt{k^I_{zmn}/k^I_{zmi}}\,(-1)^i \cdot \int_0^b \frac{\cos(n\pi z/b)}{\sqrt{1+\delta_{on}}}\,\frac{\cos\{k^I_{zmi}(z-b)\}}{\sqrt{1+\delta_{oi}}}\,dz$$

Again, the combinations $(mn,\ mi)$ are related to one matrix element. Finally, the elements of the two diagonal matrices read

$$\begin{aligned}
(\underline{D}_S)_{mn} &= \text{Diag}\,\{j/\sin(k^I_{zmn}b)\} \\
(\underline{D}_T)_{mn} &= \text{Diag}\,\{j/\tan(k^I_{zmn}b)\}
\end{aligned}$$

REFERENCES

[1] Holme, S.C., "A 12 GHz 12 channel contiguous multiplexer for satellite applications", in 1984 IEEE MTT-S Int. Microwave Symp. Dig., pp. 295-296.

[2] Tong, R. and D. Smith, "A 12-channel contiguous band multiplexer for satellite application", in 1984 IEEE MTT-S Int. Microwave Symp. Dig., pp. 297-298.

[3] Gregg, H., R.J. Brunt and M.C. Hughes, "A new generation of 12 GHz channel demultiplexers for communications satellite applications", in Proc. 17th European Microwave Conf., pp. 707 - 712, 1987.

[4] Frenna, J., "Realization of dual-mode longitudinal filters with arbitrary polarization of input and output ports", in 1986 IEEE MTT-S Int. Microwave Symp. Dig., pp. 253-256.

[5] Zaki, A.K., C. Chen, and A.E. Atia, "A new realization of dual mode dielectric resonator filters", in Proc. 17th European Microwave Conf., pp. 169-174, Sept. 1987.

[6] Kobayashi, Y. and K. Kubo, "Canonical bandpass filters using dual-mode dielectric resonators", in 1987 IEEE MTT-S Int. Microwave Symp. Dig., pp. 137-140.

[7] Shih, Y.-C., "Design of waveguide E-plane filters with all-metal inserts", IEEE Trans. Microwave Theory Tech., vol. MTT-32, pp. 695-704, July 1984.

[8] Vahldieck, R., J. Bornemann, F. Arndt, and D. Grauerholz, "Optimized waveguide E-plane metal insert filters for millimeter-wave applications", IEEE Trans. Microwave Theory Tech., vol. MTT-31, pp. 65-69, Jan. 1983.

[9] Arndt, F., J. Bornemann, D. Heckmann, C. Piontek, H. Semmerow, and H. Schueler, "Modal S-matrix method for the optimum design of inductively direct-coupled cavity filters", IEE Proceedings, vol. 133, Pt. H., pp. 341-350, Oct. 1986.

[10] Bornemann, J. and F. Arndt, "Metal insert filters with improved characteristics", IEE Proceedings, vol. 133, Pt. H., pp. 103-107, Apr. 1986.

[11] Vahldieck, R. and W.J.R. Hoefer, "Finline and metal insert filters with improved passband separation and increased stopband attenuation", IEEE Trans. Microwave Theory Tech., vol. MTT-33, pp. 1333-1339, Dec. 1985.

[12] Bornemann, J., R. Vahldieck, F. Arndt, and D. Grauerholz, "Optimised low-insertion-loss millimeter-wave fin-line and metal insert filters", The Radio and Electronic Engineer, vol. 52, pp. 513-521, Nov./Dec. 1982.

[13] Matthaei, G., L. Young, and E.M.T. Jones. Microwave Filters, Impedance-Matching Networks, and Coupling Structures. Artech House, 1980.

[14] Shigesawa, H., M. Tsuji, T. Nakao, and K. Takiyama, "Two-path cutoff waveguide dielectric resonator filters", IEEE Trans. Microwave Theory Tech., vol. 37, pp. 1105-1112, July 1989

[15] Arndt, F., I. Ahrens, U. Papziner, U. Wiechmann, and R. Wilkeit, "Optimized E-plane T-junction series power dividers", IEEE Trans. Microwave Theory Tech., vol. MTT-35, pp. 1052-1059, Nov. 1987.

[16] Knetsch, H.D., "Beitrag zur Theorie sprunghafter Querschnittsveränderungen von Hohlleitern", Arch. Elektr. Uebertr., vol. 22, pp. 591-600, Dec. 1968.

[17] Kuehn, K., "A mode-matching method for solving field problems in waveguide and resonator circuits", Arch. Elektr. Uebertr., vol. 27, pp. 511-518, Dec. 1973.

[18] Schmiedel, H., Berechnung und Messung von Diskontinuitaeten im Rechteckhohlleiter unter besonderer Beruecksichtigung der Analyse und Synthese von Modenkopplern. Fortschritt-Bericht, 9, No. 37, VDI-Verlag Duesseldorf, 1983.

[19] Bornemann, J. and F. Arndt, "Modal-S-matrix design of optimum stepped ridged and finned waveguide transformers", IEEE Trans. Microwave Theory Tech., vol MTT-35, pp. 561-567, June 1987.

[20] Bornemann, J., "A new class of E-plane integrated millimeter-wave filters", in 1989 IEEE MTT-S Int. Microwave Symp. Dig., pp. 580-583.

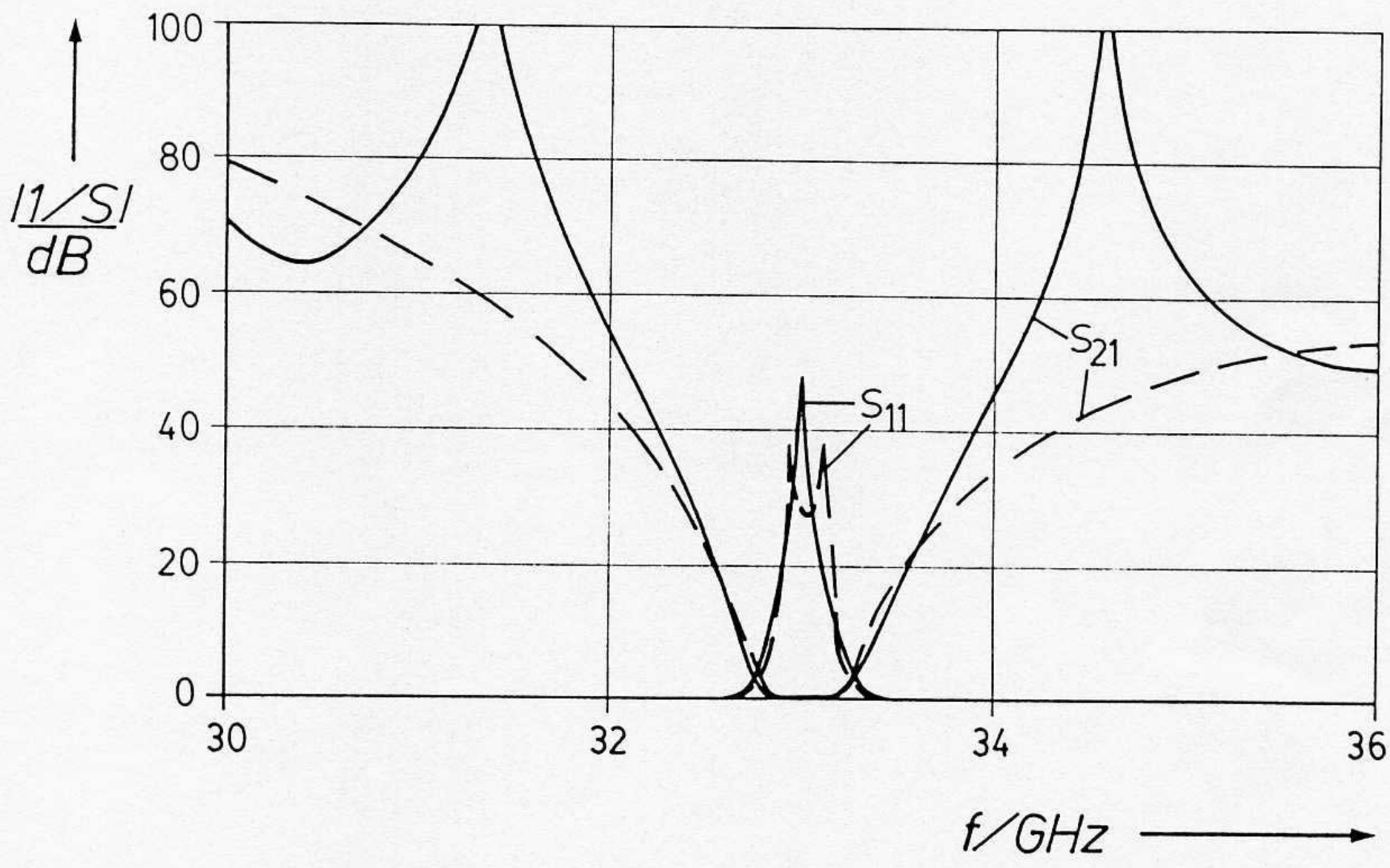

Figure 2

Optimized Ka-band filter with two identical stopband sections; solid lines: this design, dashed lines: conventional metal insert filter for comparison.

$a = 2b = 7.112$mm, $t = 127\mu$m, $d_1 = d_4 = 10.921$mm, $d_2 = d_5 = 0.16$mm, $d_3 = d_6 = 7.365$mm, $\ell_0 = \ell_8 = 9.086$mm, $\ell_1 = \ell_7 = 1.561$mm, $\ell_2 = \ell_6 = 4.198$mm, $\ell_3 = \ell_5 = 4.875$mm, $\ell_4 = 4.202$mm.

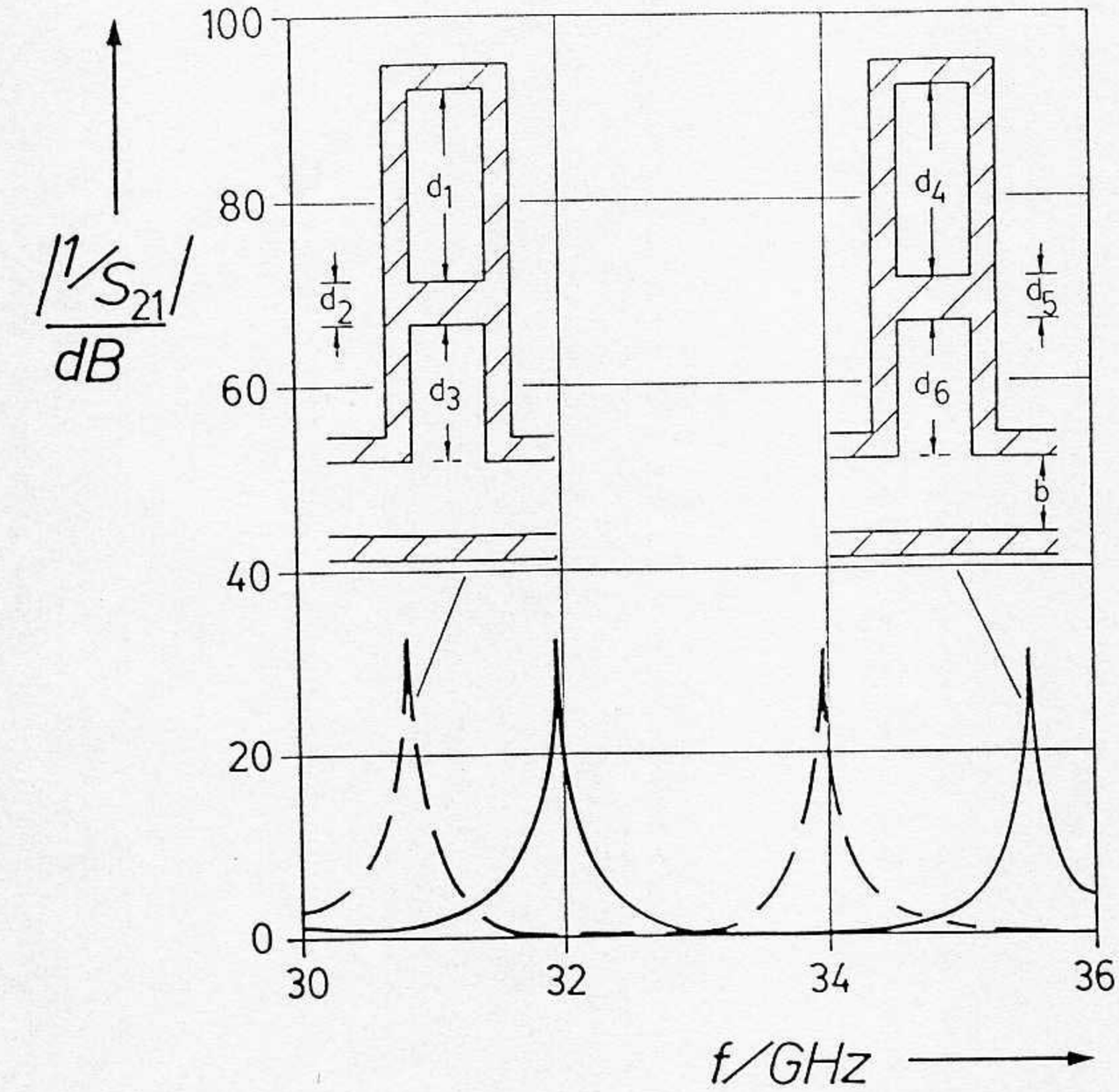

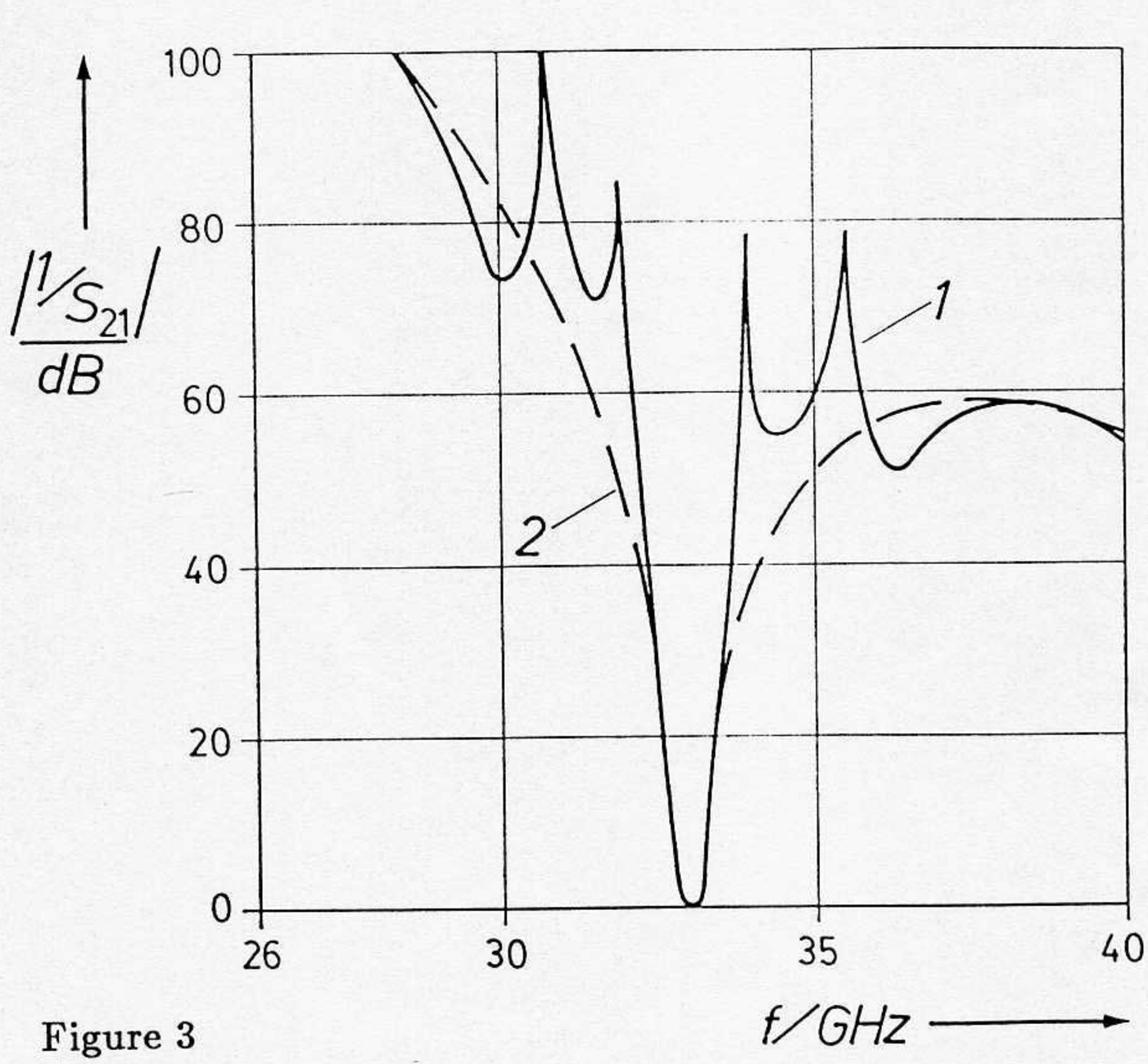

Figure 3

Optimized Ka-band design comprising different stopband sections; top: response of stopband circuits only; bottom: insertion loss of the complete filter structure (1) and a conventional filter (2) for comparison.

$a = 2b = 7.112$mm, $t = 127\mu$m, $d_1 = 11.232$mm, $d_2 = d_5 = 0.13$mm, $d_3 = 7.676$mm, $d_4 = 10.537$mm, $d_6 = 6.981$mm, $\ell_0 = \ell_8 = 9.286$mm, $\ell_1 = \ell_7 = 1.501$mm, $\ell_2 = \ell_6 = 4.198$mm, $\ell_3 = \ell_5 = 5.175$mm, $\ell_4 = 4.202$mm.